COMPDYN 2011
III ECCOMAS Thematic Conference on
Computational Methods in Structural Dynamics and Earthquake Engineering
M. Papadrakakis, M. Fragiadakis, V. Plevris (eds.)
Corfu, Greece, 25–28 May 2011

FINITE ELEMENT MODELLING OF YIELDING SHEAR PANEL DEVICE FOR PASSIVE ENERGY DISSIPATION

Md Raquibul Hossain [1], Mahmud Ashraf [2], and Faris Albermani [3]

[1] School of Civil Engineering, The University of Queensland
St Lucia, QLD 4072, Australia
md.hossain@uqconnect.edu.au

[2] School of Civil Engineering, The University of Queensland
St Lucia, QLD 4072, Australia
m.ashraf@uq.edu.au

[3] School of Civil Engineering, The University of Queensland
St Lucia, QLD 4072, Australia
f.albermani@uq.edu.au

Keywords: Earthquake, Finite Element Method, Shear deformation, Passive Energy Dissipation, Yielding Shear Panel Device.

Abstract. *Yielding Shear Panel Device (YSPD) is a newly proposed passive energy dissipation device to make structures more sustainable against earthquakes by exploiting the shear deformation capacity of metallic plates. YSPD is easy to install using simple bolted connections and is significantly less expensive than currently available passive energy dissipation devices. If required, damaged YSPDs could be replaced easily after an earthquake causing minimum disruption to a structure. The current research explains the development of finite element models for the pilot experiments carried out on YSPD. The developed FE models include both material and geometric nonlinearities and use nonlinear spring elements to model appropriate support conditions observed in the experiments. Overall, good agreement is noticed between the FE models and the test results in regards to force displacement response and energy absorption. The developed FE models are validated for both monotonic and cyclic loading. This verification paves the way for generating further reliable set of data to develop appropriate design rules for YSPD.*

1 INTRODUCTION

Recent catastrophic earthquakes occurring in different parts of the world demonstrate the severity of this natural phenomenon on human civilization and points out the significance of further research to develop efficient cost-effective tools to minimise the resulting loss. Minimization of structural damages due to earthquake is a major area of research which contributed to the development of a number of active, semi-active and passive control mechanisms during the last few decades. The current research investigates the structural performance of a newly proposed yielding shear panel device (YSPD) for passive energy dissipation. YSPD is very simple to manufacture and is economical when compared against currently available devices. Pilot tests carried out on the device demonstrates its potential for considerable energy absorption [1]. Appropriate design rules for YSPD would require more understanding of its structural response when subjected to different types of loading. Finite element models are developed herein and verified against available monotonic and cyclic test results to pave the way for thorough parametric analysis leading to design rules. The scope of this paper covers details of the FE modelling technique using the general purpose FE package ANSYS.

2 YIELDING SHEAR PANEL DEVICE (YSPD)

Diagonal tension field that develops in the post-buckling regime of a thin steel plate under shear, which offers significant strength and ductility, can be utilized to dissipate energy. This concept led to the development of a new metallic passive energy dissipating device 'Yielding Shear Panel Device' (YSPD). YSPD was introduced by Williams and Albermani [2] based on the proposed design by U. Dorka at the University of Kassel, Germany to exploit the energy dissipative capability of steel plates through in-plane shear deformation and the concept was further explored by Schmidt et.al. [3] and Williams and Albermani [4]. YSPD relies on the in-plane shear deformation of a thin diaphragm steel plate welded inside a square hollow section (SHS). This device can be placed below a structural beam using a V-brace, as shown in Figure 1, so that it automatically comes into play in the event of any horizontal excitation.

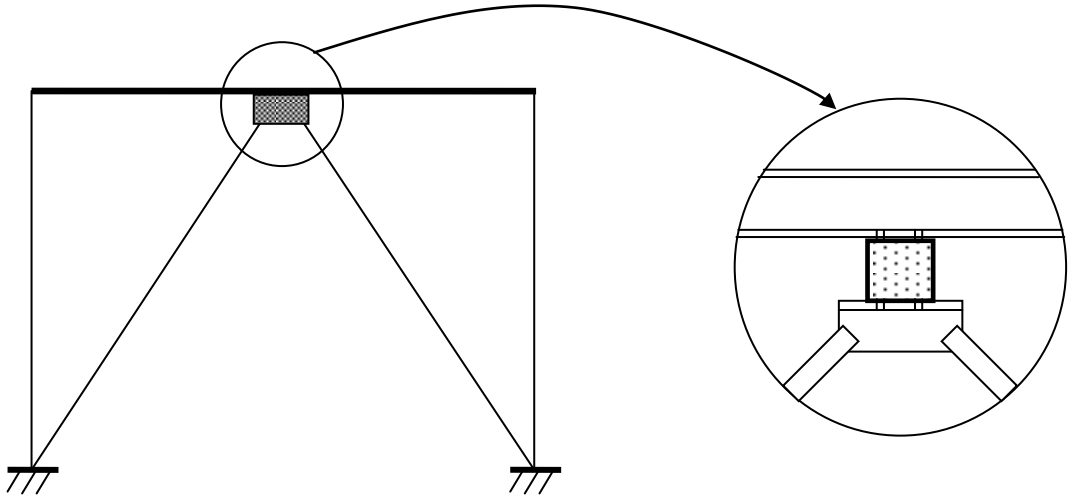

Figure 1: Typical YSPD-brace assembly.

Chan et. al. [1] conducted a series of monotonic and cyclic tests using various plate thicknesses and device configurations for YSPD. The tested specimens were fabricated using a short segment of a square hollow section (SHS) with a steel diaphragm plate welded inside it as shown in Figure 2. Four bolt holes spaced at a centre-to-centre distance 's' were drilled on

each of the two opposite SHS flanges for connecting the device to the test setup; this connection is analogous to the practical assembly where YSPDs are proposed to be connected using bolts to ensure easy installation and replacement. The SHS provides a boundary to the diaphragm plate so that shear forces can be applied to the plate, in addition to providing necessary detail for connections to the parent structural frame. Most importantly, the SHS serves as a boundary element allowing the tensile strips to be formed and the tension field to be developed following the post-buckling of the thin diaphragm plate. As a result of sufficiently large displacements occurring in the diaphragm plate, the input energy originating from an earthquake could be dissipated through plastic deformation.

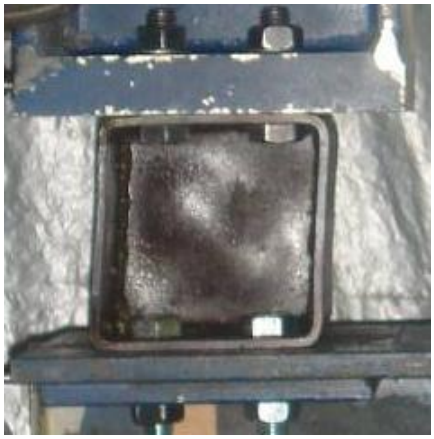

(a)

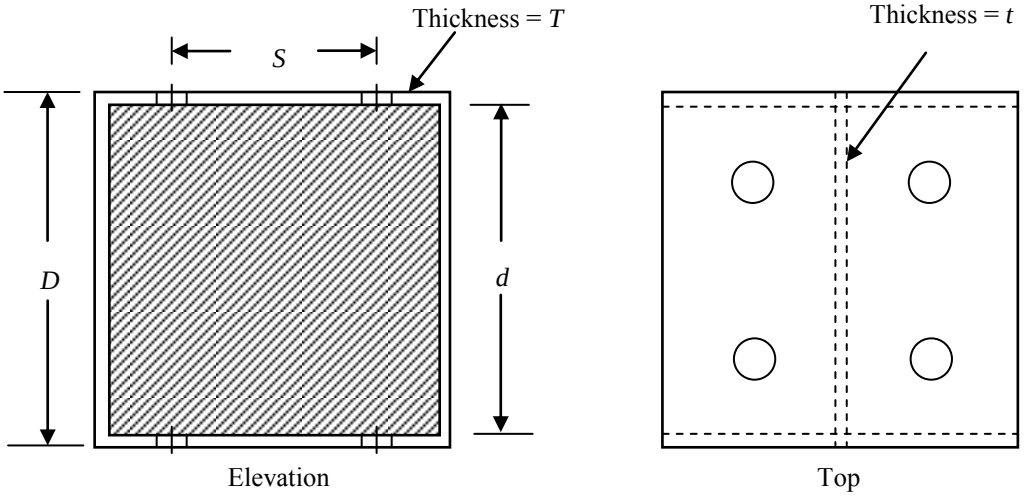

(b)

Figure 2: (a) Yielding shear panel device (YSPD) (b) Schematic diagram showing the geometric parameters of YSPD [5].

Chan et. al. [1] tested two different sizes of YSPD, 100mm × 100mm and 120mm × 120mm, with three different thickness of 2 mm, 3 mm and 4 mm for the diaphragm plate. Bolt spacing of 50 mm was used for four M16 bolts on each side of the SHS to install the test specimen between a ground beam and L-beam. Geometric dimensions of the test specimens are given in Table 1 and reported material properties are summarized in Table 2.

YSPD Designation (D × D × t)	Diaphragm Thickness, t (mm)	SHS Size, D (mm)	SHS Thick-ness, T (mm)	Bolt Spacing, S (mm)
100×100×2	1.86	100	3.76	50
100×100×3	2.83	100	3.76	50
100×100×4	3.78	100	3.76	50
120×120×2	1.86	120	4.91	50
120×120×3	2.83	120	4.91	50
120×120×4	3.78	120	4.91	50

Table 1: Geometric details of YSPD test specimens [1]

YSPD Designation (D × D × t)	Tensile Yield Strength (MPa)	
	Diaphragm Plate	SHS
100×100×2	211.3	414.9
100×100×3	321.3	414.9
100×100×4	351.2	414.9
120×120×2	211.3	333.3
120×120×3	321.3	333.3
120×120×4	351.2	333.3

Table 2: Material properties of the test specimens [1]

3 FINITE ELEMENT MODELLING OF YSPD

3.1 Material modelling

An appropriate material model is a prerequisite to obtain accurate predictions from a finite element model. Williams and Albermani [4] and Chan et. al. [1] used ordinary carbon steel plates and steel SHS sections to manufacture the tested YSPD specimens. Stress-strain response of ordinary steel shows a steep initial elastic response followed by strain hardening up to the ultimate stress followed by strain softening before failure. Most widely adopted material modelling technique for carbon steel is, however, the bilinear elastic, perfectly-plastic idealization. Alinia et. al. [6] recently used bilinear hardening model to analyze the plastic shear buckling capacity of unstiffened steel plates. Eurocode 3 [7] provides the following guideline for assuming the bilinear material behaviour – material behaviour can be modelled without strain hardening, with a nominal plateau slope or with linear strain hardening depending on the accuracy and the allowable strain required. The Code suggests that the tangent modulus after yielding can be reasonably assumed as 1% of the Young's modulus of elasticity for a bilinear idealization to include the effects of strain hardening. Chan [5] reported two coupon tests for the 100×100×4 SHS. Figure 3 compares the reported coupon test results and

the idealized bilinear material model. Young's modulus of elasticity E = 200 GPa and Poission's ratio ν = 0.3 for mild steel is used in material modelling.

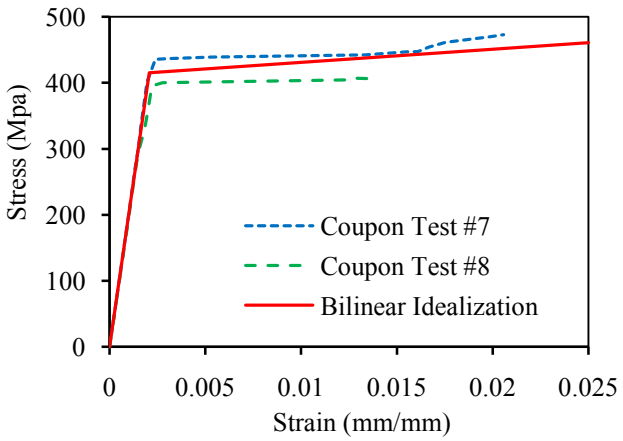

Figure 3. Material properties of the SHS plate of YSPD 100x100x4 [5]

An isotropic hardening model may be used to simulate the material behaviour only for monotonic loading, whilst cyclic behaviour would require a kinematic hardening model as the yield surface can translate in the direction of loading. A bilinear kinematic hardening model available in ANSYS assumes that the total stress range as twice the yield stress which eventually results in von Mises yield criteria with an associative flow rule. The yield surface is assumed to have a cylindrical shape in three-dimensional stress space as shown in Figure 4. This model represents the stress-stain response in two stages – the initial linear elastic part where the material follows the Hook's law and in the following linear plastic part where the material exhibits a constant strain hardening behaviour. The bilinear kinematic hardening model is used in the current study as the constitutive model for the steel plates used in the diaphragm plate as well as the SHS of YSPD for both monotonic and cyclic loading.

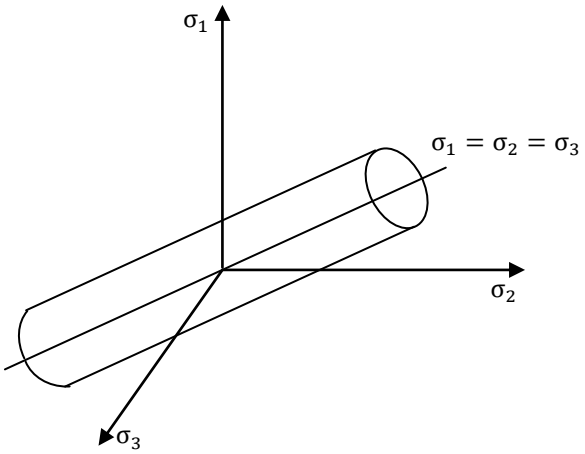

Figure 4: von Mises yield surface in the three-dimensional stress space.

3.2 Analysis technique and selection of element type

Developed FE models were analysed elastically to obtain appropriate Eigenmodes, which were used to model initial geometric imperfections in the subsequent nonlinear analysis. The 'BUCKLE' option available in ANSYS was used to obtain the required Eigenmodes followed

by a nonlinear 'STATIC' analysis to simulate the force-displacement response of YSPD. To take appropriate account of the geometric nonlinearity effects arising as a result of excessive deformation of the thin diaphragm plate, the 'NLGEOM' option was adopted.

A number of techniques for solving the global system of simultaneous equations are available in the ANSYS program such as sparse direct, preconditioned conjugate gradient (PCG), Jacobi conjugate gradient (JCG), frontal direct etc. Among these available options, PCG solver is an iterative equation solver that can handle ill-conditioned problems and provide faster solution for large models when compared against the performance of sparse and frontal solvers. Line search option, accessed with 'LNSRCH' command, can further improve the performance of the solution technique [8]. The current FE modelling uses PCG solver with the line search option to obtain an accurate response of YSPD, whilst minimising computational time.

Shell elements are widely used to model thin-walled structures. In recent times, Alinia et. al [6] used four noded quadrilateral shell elements to investigate the plastic shear buckling capacity of unstiffened steel plates, whilst De Matteis et. al. [9] employed shell elements to model stiffened aluminium shear panels. Soo Kim and Kuwamura [10], Ashraf et. al. [11], Ellobody and Young [12] used general purpose shell elements to analyze the behaviour of thin-walled stainless steel members. ANSYS offers a range of shell elements including both general purpose and special purpose elements. 'SHELL43' and 'SHELL181' are two general purpose shell elements suitable for thin to moderately thick shell structures incorporating nonlinear, large deflection and large strain capabilities. Special purpose shell element 'SHELL41' is a membrane only element having only membrane stiffness, whilst 'SHELL63' is an elastic shell element. General purpose shell element 'SHELL181' is used in the current research to model both the diaphragm plate and the SHS. 'SHELL181' is a four-noded full integration quadrilateral shell element with six degrees of freedom at each node, which is well-suited for linear, large rotation, and/or large strain nonlinear applications [8]. It includes both bending and membrane stiffnesses.

3.3 Support conditions for YSPD

Modelling appropriate support conditions for YSPD has been one of the challenging tasks in the current research as it significantly affects the overall load-deformation response and the amount of dissipated energy. The current proposal is to connect YSPD to the parent structure using bolts to ensure easy installation and to facilitate replacement of damaged devices after an earthquake, if required.

3.3.1. Stiffness of the SHS

Chan et al. [1, 5] installed the test specimens between a ground beam and an L-beam, securely fastened by four M16 bolts on each side.. The left flange of the YSPD was connected to the ground beam, whilst the right flange was connected to the L beam. Forced displacements were applied using a 100kN capacity MTS actuator to the YSPD through the L-beam, which moved vertically downward and upward to simulate the horizontal displacement that would occur in a V-brace assembly due to an earthquake excitation.

Displacement measurements obtained from LVDT 2 and LVDT 3 showed some initial in-plane rotation of the L-beam (Figure 5a). Considerable deformations were observed in YSPD specimens. The upper flange of the YSPD moved rightward, whilst the lower flange moved leftward due to this in-plane rotation of the L-beam caused by the downward movement of the actuator. These movements caused the support end flange (left flange) and the loading end flange (right flange) to experience bending in upper and lower portions respectively. The up-

per two bolts of support end and the lower two bolts of loading end experienced minor deformations due to this bending. Opposite movements and deformations were observed when the actuator moved upwards. Figure 5(b) shows the deformed shape for YSPD 100×100×3 after the monotonic test. Noticeable bending observed at the flanges is highlighted by circles.

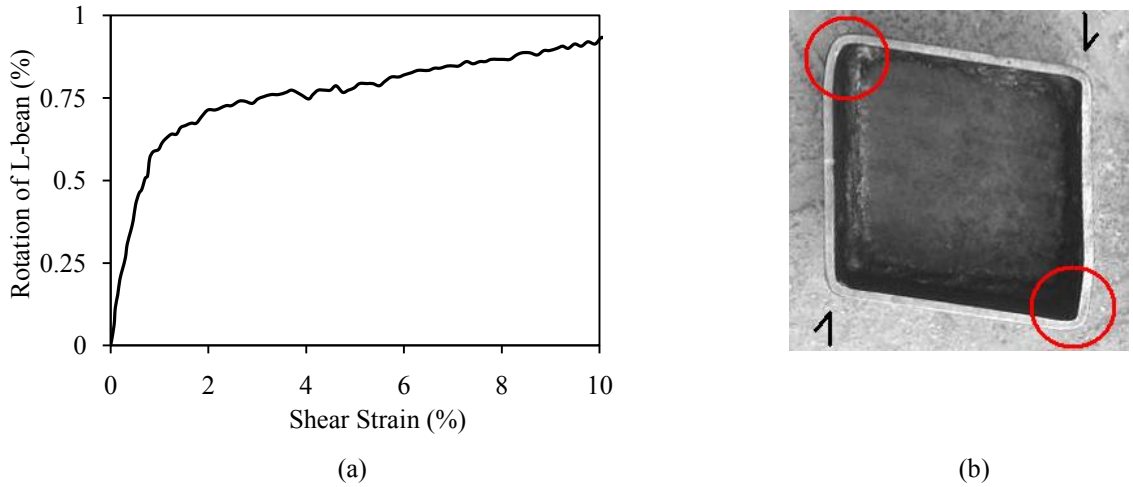

Figure 5: (a) In-plane rotation of the L-beam of YSPD 100X100X3 under monotonic loading (b) Deformed shape of YSPD 100X100X3 under monotonic loading [5]

3.3.2. FE modelling of the boundary conditions

The developed FF models of the YSPD have the same orientation that would occur when YSPD will be placed in a V-brace assembly (Figure 6). In actual practice the upper flange will be connected to the beam, whilst the bottom flange will be connected to the V-brace. Both the upper and the lower bolted flanges will experience bending due the horizontal movement of the V-brace, which is simulated by applying horizontal nodal displacements to the nodes around the bolt holes of the lower flange. Bolts nearer to the bent flange plates will experience minor deformations due to bending effects originating from these movements. The other two edge lines are supported by the beam and the V-brace end plate.

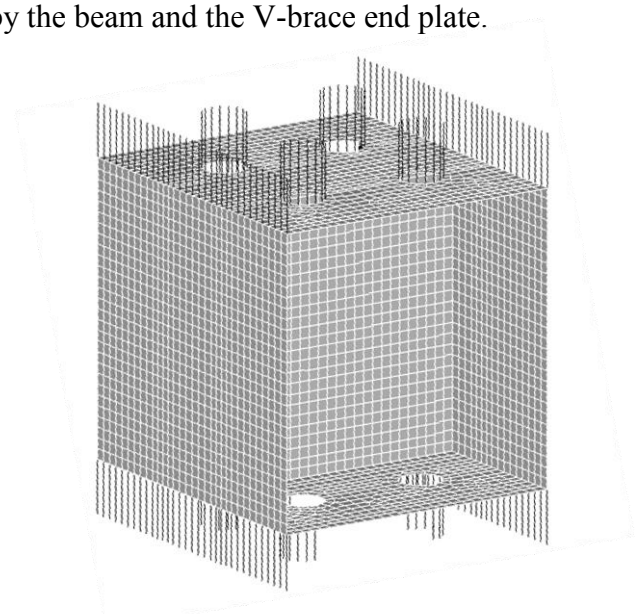

Figure 6: Spring elements (ANSYS) used to model appropriate boundary conditions for YSPD.

The deformations and movements observed in the bolts and the edges of YSPD were modelled using a combination of hinge and spring supports as shown in Figure 6. All nodes along four edge lines are supported by 'COMBIN39' spring elements, which act as a tension-compression element. Both tension and compression will occur due to the bending effects resulting from horizontal movements. Tension and compression stiffnesses are defined separately to allow the elements exhibit different force-displacement responses in tension and compression. The compression stiffness K_{ec} of the edge springs are taken equal to the stiffness of the flange plate. The cross-sectional area between two nodes constitutes the stiffness for a single spring. These springs resist the edge nodes to move beyond the support and the loading planes. The stiffness for the edge springs at the loading side is reduced by multiplying with a reduction factor λ to incorporate the effects of in-plane rotation observed at the loading side. The tension stiffness K_{et} is taken as a very small positive magnitude to eliminate the numerical singularity that allows the edge nodes to move freely in both directions but resists them to go away from the support and the loading planes.

Bolted connections are simulated using circular holes with appropriate boundary conditions around the perimeter. The nodes around the circular hole are divided into two categories - inner nodes and outer nodes as shown in Figure 7. At the support end, the translational degrees of freedom for the inner nodes are fully restrained, whilst the outer nodes are restrained only against the in-plane movements. To simulate the out of plane displacements, these nodes are supported by 'COMBIN39' spring elements with stiffness (K_b) whose combined stiffness is equal to the stiffness of the M16 bolts as used in the experiment. At the loading end, both the inner and the outer nodes are supported by 'COMBIN39' spring elements with stiffness equal to a fraction of the stiffness of M16 bolts λK_b. These nodes are free against in-plane displacements to simulate the observed horizontal movement of the V-brace end plate during testing. Table 3 presents a summary of the magnitudes of appropriate stiffness for spring supports used at the support and at the loading end.

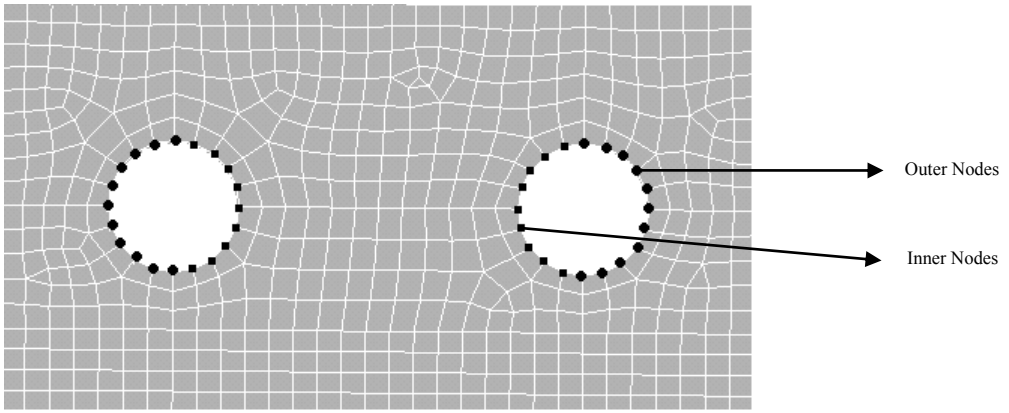

Figure 7: Definition of inner and outer nodes around the bolt hole.

	Stiffness
Tensile stiffness of the edge springs, K_{et}	0.0001
Compressive stiffness of the edge springs, K_{ec}	$T \times S_n \times E_{SHS}$
Stiffness of the springs at bolt holes, K_b	$\frac{A_b \times E_b}{N_b}$

Table 3: Spring stiffness values used for modelling boundary conditions of YSPD.

Where,

T = Thickness of the SHS plate
S_n = Nodal spacing in the SHS plate
E_{SHS} = Modulus of elasticity of SHS plate
A_b = Cross section area of bolt
E_b = Modulus of elasticity of bolt
N_b = Number of nodes per bolt hole

The reduction factor λ allows the in-plane rotation and degradation of the initial stiffness of YSPD, which are inevitable phenomenon as observed during testing (Figure 5a). The rotation at the loading end is significantly affected by the value of λ; a higher value of λ contributes to a smaller rotation. The support end and the loading end will be parallel if λ is taken as 1.0; this will eventually make the initial stiffness of the YSPD equal to that proposed by Chan et. al. [1]. The test results, however, show a significantly lower initial stiffness as a result of the observed rotation at the loading end.Test results showed noticeable in-plane rotation of the L beam despite its high stiffness. A parametric study was conducted to find an appropriate value for λ. Figure 8 shows the load-deformation responses of YSPD for different values of λ against test results. Comparisons show that only a small fraction of K_b and K_{ec} produces good agreement with test results and hence a value of λ = 0.002% has been adopted in the current research to allow for the in plane rotation.

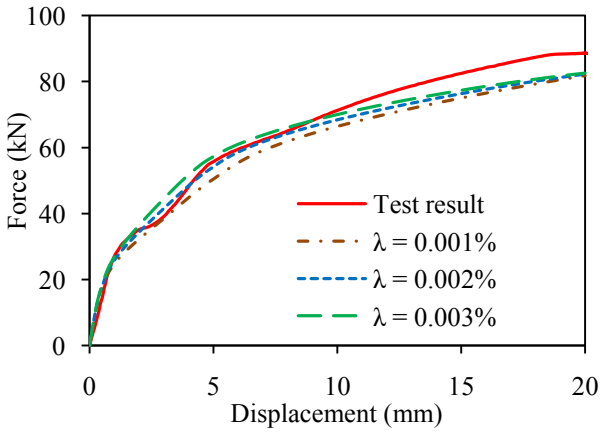

Figure 8: Load-deformation response of YSPD 100×100×4 with different values for λ.

3.4 Convergence study – selecting a suitable mesh

Selecting an appropriate mesh is one of the most important aspects of FE modelling. No general guidelines are available to choose a suitable mesh as it largely depends on the type of structure and the corresponding analysis involved. Finer mesh generally provides better predictions but require higher computational time. A convergence study was carried out to choose a suitable mesh to obtain an optimum balance between accuracy and computational time.

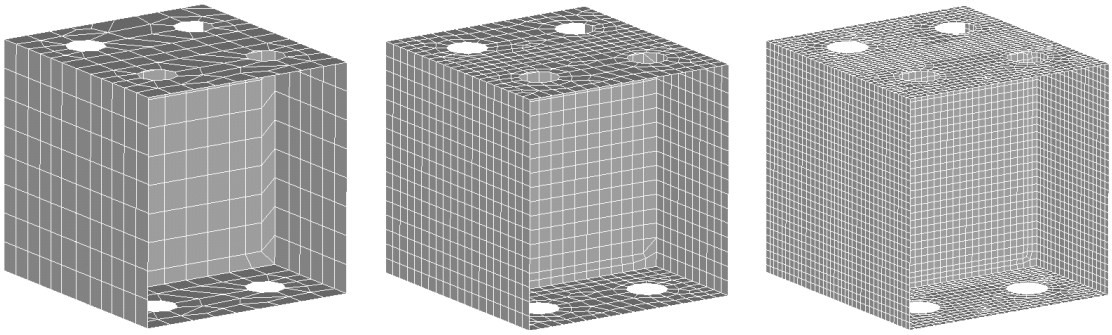

(a) (b) (c)

Figure 9. Convergence study of YSPD (100×100×4). (a) Coarse mesh (492 shell elements), (b) Medium mesh (1516 shell elements), (c) Fine Mesh (5238 shell elements)

Three different mesh sizes were used to simulate the load-deformation response of YSPD as shown in Figure 9. The size of element in the finer mesh was half of the size of medium mesh and one-fourth of the size of coarse mesh. Fig 10 shows a typical force-displacement response for different mesh densities. Results showed that both the finer mesh and the medium mesh give reasonable agreement with test result. No further refinement was attempted since the predictions were found to be in line with the test results and the finer mesh has been adopted in subsequent finite element models to ensure better accuracy.

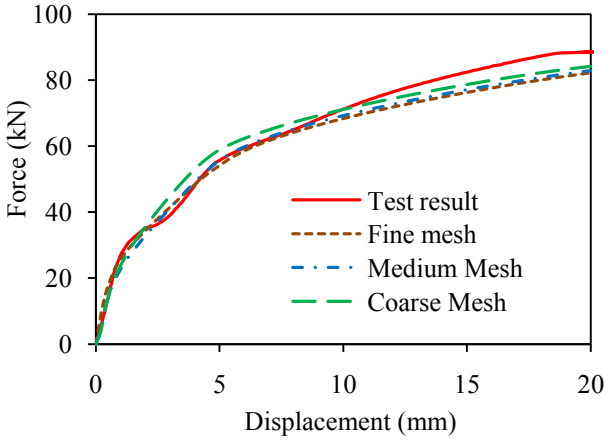

Figure 10: Typical force-displacement response due to different mesh sizes (YSPD 100×100×4)

3.5 Initial Imperfections

Yielding shear panel device consists of two main parts – a steel diaphragm plate and a square hollow section (SHS). The diaphragm plate is placed inside the SHS at mid depth and welded along the four sides of the diaphragm plate; this process induces residual stresses. In addition, the steel plates used to fabricate YSPD are not perfectly plane as they always inherit some geometric imperfections i.e. out-of-plane deformations. Effects of geometric imperfections and residual stresses are, therefore, investigated in this section as part of the FE modelling of YSPD.

3.5.1. Geometric Imperfections

Initial geometric imperfections are an inevitable property of steel structures because of the typically high width-to-thickness ratio, which influences their structural response. The impor-

tance of modelling initial imperfections attracted attention amongst researchers during the last few decades. In spite of its observed significance, there is no general guideline to model the magnitude and distribution of the initial geometric imperfections, largely due to the high degree of uncertainty associated with its formation process. Generally, an assumed shape and magnitude for the out-of-plane deformation is incorporated or an assumed transverse force is applied to simulate the effects of initial geometric imperfections. In recent times, the most commonly used technique for modelling imperfection distributions is either to adopt a sinusoidal wave or to use one of the Eigenmodes obtained from elastic buckling analysis; a number of recent approaches adopted for modelling thin-walled structural elements are discussed below.

Dawson and Walker [13] studied the geometric imperfections of cold-formed steel cross-sections and proposed the following relationships for geometrically imperfect plates with free edges under compression and bending,

$$\omega_0 = \alpha t \tag{1}$$

$$\frac{\omega_0}{t} = \beta \left(\frac{\sigma_y}{\sigma_{cr}}\right)^{0.5} \tag{2}$$

$$\frac{\omega_0}{t} = \gamma \left(\frac{\sigma_y}{\sigma_{cr}}\right) \tag{3}$$

Where, ω_0 is the amplitude of initial imperfection, t is the thickness of the plate, σ_y is the material yield stress, σ_{cr} is the critical plate buckling stress, whilst α, β and γ are constants. In addition, a conservative fit of the maximum imperfection amplitude was reported to be equal to 0.2t. Gardner [14] adopted Equation 7 with a proposed value of $\gamma = 0.023$ for roll-formed stainless steel hollow sections under compression and used the 1st Eigenmode for imperfection distribution.

Schafer and Pekoz [15] proposed the following two simplified regression based relationships to determine the imperfection amplitude ω_0 for cold formed steel lipped channel sections and assumed that the magnitude of imperfections in the lowest Eigenmode is sufficient to characterize the influence of imperfections. In the first formulation, the imperfection amplitude is linearly varied with the width (w) as follows,

$$\omega_0 = 0.006w \tag{4}$$

The second formulation is based on an exponential curve fit to the plate thickness as,

$$\omega_0 = 6te^{-2t} \tag{5}$$

EN 1993-1-5 [7] recommends to apply the equivalent local geometric imperfection for finite element models panels or sub panels based on the shape of the critical plate buckling modes with amplitude of w/200, which is linearly proportional to the minimum dimension of the panel. It gives lower imperfection magnitudes than Schafer and Pekoz's [15] proposed Equation 8.

Zhang et.al. [16] measured the maximum imperfections observed in cold formed steel channel columns and the obtained magnitudes varied from 0.03t to 0.25t, whilst the distribution of imperfections showed reasonable resemblance with the 1st Eigenmode. Sun and Butterworth [17] used imperfection magnitude of 0.167t, 0.333t, 0.5t and 0.667t to model the behaviour of steel single angle compression members eccentrically loaded through one leg; the use of amplitude 0.333t produced best predictions. Pokharel and Mahendran [18] investigated the sensitivity of imperfection for sandwich panels by varying the amplitude between 0.1t and 0.4t. The 1st Eigenmode was used to model imperfection distribution in all cases; the overall effect on the ultimate compressive strength was observed to be insignificant. Pavlovcic et.al. [19] investigated the reduction in shear resistance of longitudinally stiffened panels due to a range of local and global geometric imperfections within the prescribed limit according to EN 1993-1-5 [7]. Global imperfections were defined using the stiffener out-of-

plane deflections in half-sine wave, whilst local imperfections in sub panels were modelled with critical local buckling modes for panels with trapezoidal stiffeners. Results obtained using combined imperfections showed that the reduction in panel shear resistance capacity has a small influence due to imperfections. Ashraf et.al. [11] reported a detailed review of different techniques adopted for modelling geometric imperfections observed in thin-walled structural components. The degree of uncertainty associated with geometric imperfections make it almost impossible to come up with a generalised formulation which can be adopted directly in FE modelling.

The current research adopts the most commonly used technique of obtaining Eigenmodes through elastic buckling analysis of the developed FE model, which are subsequently used as the initial shape in nonlinear analysis. Figure 11 shows some typical Eigenmodes of YSPD obtained through elastic buckling analysis. The distribution of the initial geometric imperfections is assumed to have the same shape as one of the obtained Eigenmodes. In ANSYS, the nodal displacements of an Eigenmode are normalised using the maximum displacement that occurs within a structure and thus the maximum displacement is set equal to unity. By specifying an appropriate multiplying factor, which is the maximum magnitude of imperfection, the nodal co-ordinates are scaled accordingly. This magnitude of the maximum initial geometric imperfection, commonly known as amplitude, is generally taken as a fraction of the plate thickness. A parametric study has been conducted to identify a suitable distribution and the corresponding amplitude of initial geometric imperfection. Figure 12 shows typical force-displacement response for variation in imperfection amplitude and distribution. Obtained results showed insignificant effect of initial geometric imperfections on the force-displacement response of YSPD. Diagonal tension in the diaphragm plate makes the incorporated initial imperfections less effective when compared to its significance in other types of loading e.g. members subjected to longitudinal compression. In the current research, the 1st Eigenmode is used to define the distribution of initial imperfections as this normally represents the lowest buckling capacity. An amplitude of 0.2t, where t is the thickness of the diaphragm plate, has been used to obtain a reasonable imperfection distribution for YSPD.

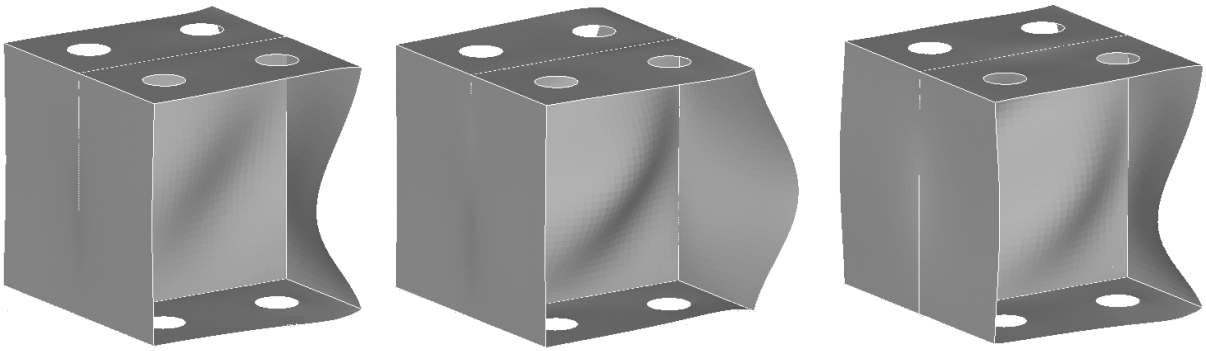

Figure 11: Eigenmodes 1, 2, and 3 for YSPD 100×100×4 obtained through elastic buckling analysis.

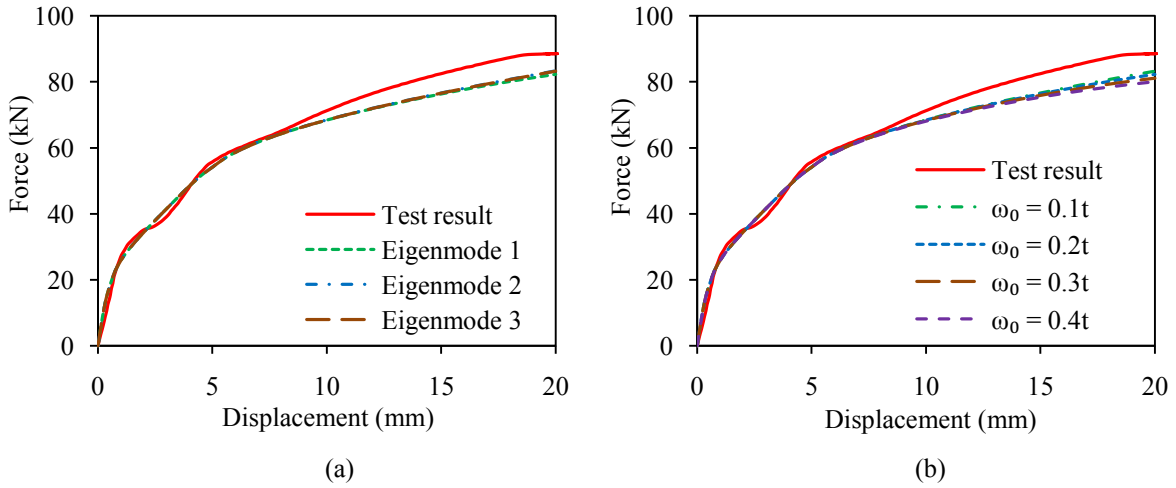

Figure 12: (a) Typical force-displacement responses of YSPD (100×100×4) as a result of using different imperfection distributions (Eigenmodes) for imperfection amplitude, $\omega_0 = 0.2t$, (b) Typical force-displacement responses due to different imperfection magnitude (ω_0) for the 1st Eigenmode.

3.5.2. Residual stresses

High thermal gradient involved in the welding process induces residual stresses; the magnitude and distribution of residual stresses are, however, quite complex in nature. Masubuchi [20] reported an extensive review on the distribution of residual stresses in different welded shapes. Odar et.al. [21] investigated the magnitude and distribution of residual stresses due to welding process on H and T sections using a method of sectioning, whilst Murugan et.al. [22] measured residual stresses in welded Tee-joint using contour method. Cruise and Gardner [23] conducted experiments for determining imperfections in long austenitic stainless steel sections and proposed simple predictive tools for both local and global imperfections. All experimental results show that tensile residual stress is induced nearer to the welded region, whilst compressive residual stresses are present in the remaining part of the cross-section.

Although the actual distribution of residual stresses is somewhat complicated, a number of simplified guide lines have been proposed by researchers. ECCS publication no. 33 [24] presents a simplified method to model thermally induced residual stresses for welded I sections – the tensile stresses nearer to the welded region and the compression stresses in the other part of the plate are assumed to have trapezoidal distributions. The magnitude of the tensile stress is assumed equal to the yield strength, whilst that for the compressive stress is equal to 25% of the yield strength; the resultant of the tensile and compressive stresses is self-balanced. Ueda et.al. [25] proposed a more simplified rectangular distribution for residual stresses in welded square plates. Liang et.al. [26] adopted the rectangular stress block approach to model residual stresses in concrete-filled welded steel box columns.

In the case of YSPD, a thin diaphragm steel plate is welded inside a square hollow section (SHS). The welding process induces residual stresses both in the diaphragm plate and the square hollow section. To investigate the effects of this residual stress, a simplified rectangular stress distribution is assumed with the magnitudes taken following ECCS specification i.e. the tensile stress is set equal to the yield strength, whilst the compressive stress is taken as 25% of the yield strength. The details are given in Figure 13. The force-displacement responses obtained for YSPDs with and without residual stresses are compared in Figure 14, which shows that residual stresses have negligible effect on the force-displacement response. Residual stress is incorporated for the exact finite element modelling of YSPD though it has an insignificant effect.

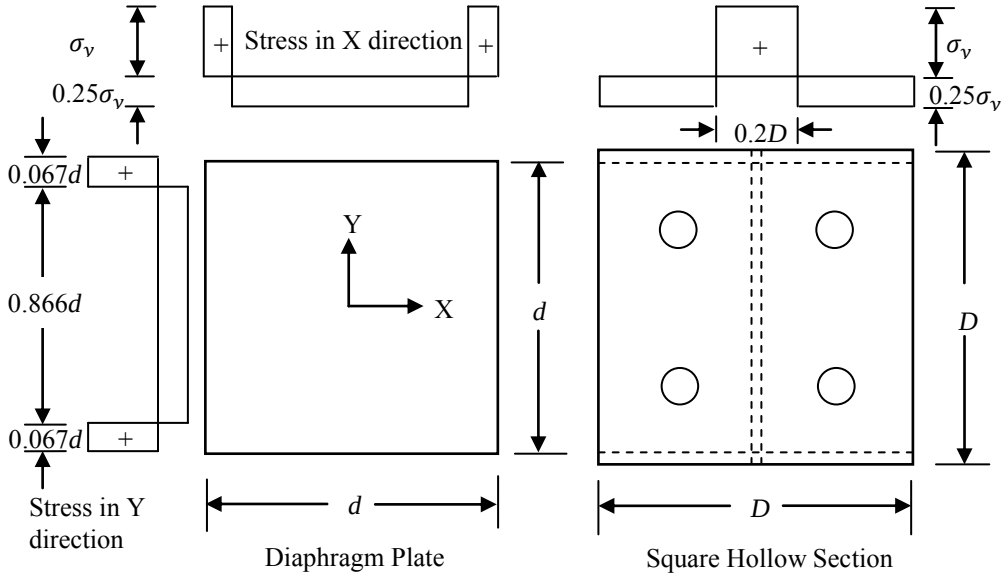

Figure 13: Residual stress Distribution in YSPD

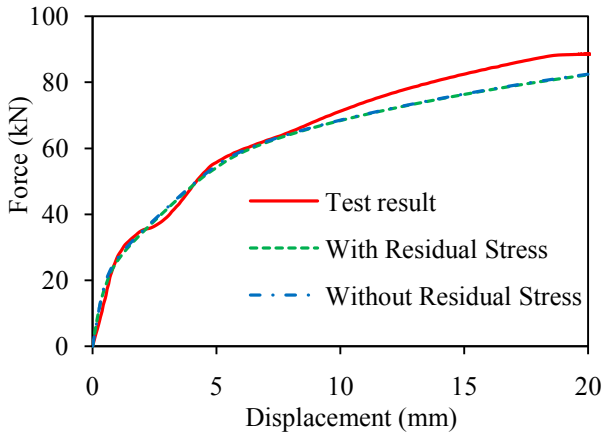

Figure 14: Typical force-displacement response with and without residual stress (YSPD 100×100×4)

4 LOAD-DEFORMATION RESPONSE OF YSPD UNDER MONOTONIC LOADING

A finite element model is developed for yielding shear panel device. Figure 15 compares the force-deformation response of YSPDs obtained from test results to those obtained from FE simulation. The devloped FE model with 2 mm diaphragm plate significantly underpredicts the test behaviour; this discrepancy is due to a higher strength shown by the material after a low yield strength (211.3 N/mm^2).

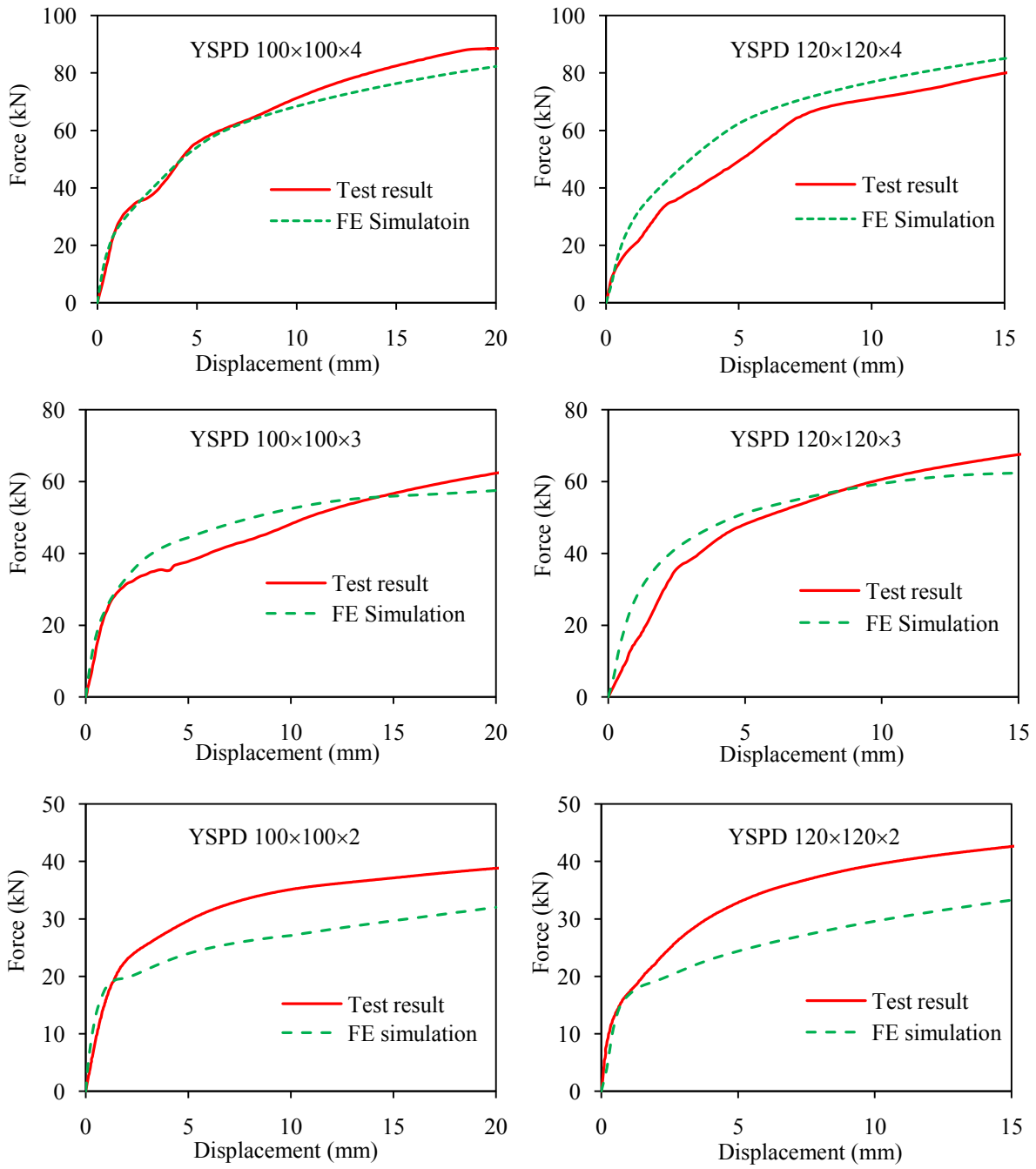

Figure 15. Force-displacement responce of YSPDs.

Table 4 compares the amount of energy required to achieve specified displacements during the monotonic loading tests of YSPDs to those obtained from finite element simulation. The ratio of energy required for different displacements indicates that the developed finite element models can predict the required energy with reasonable accuracy.

YSPD Designation	Ratio of Energy for different displacements (FE/Test)			
(D ×D×t)	5 mm	10 mm	15 mm	20 mm
100×100×2	0.89	0.83	0.81	0.81
100×100×3	1.13	1.14	1.09	1.05
100×100×4	1.01	0.99	0.97	0.95
120×120×2	0.81	0.77	0.77	-
120×120×3	1.22	1.09	1.03	-
120×120×4	1.29	1.17	1.13	-

Table 4: Comparison of energy required in monotonic loading.

5 LOAD-DEFORMATION RESPONSE OF YSPD UNDER CYCLIC LOADING

Developed FE models were subjected to cyclic loading to validate their accuracy so that reliable results could be generated to develop design rules for YSPD. Figure 16 shows the force-displacement response of YSPDs when subjected to a displacement controlled cyclic loading. Cyclic response, overall, shows a good correlation between the test results and finite element simulation.

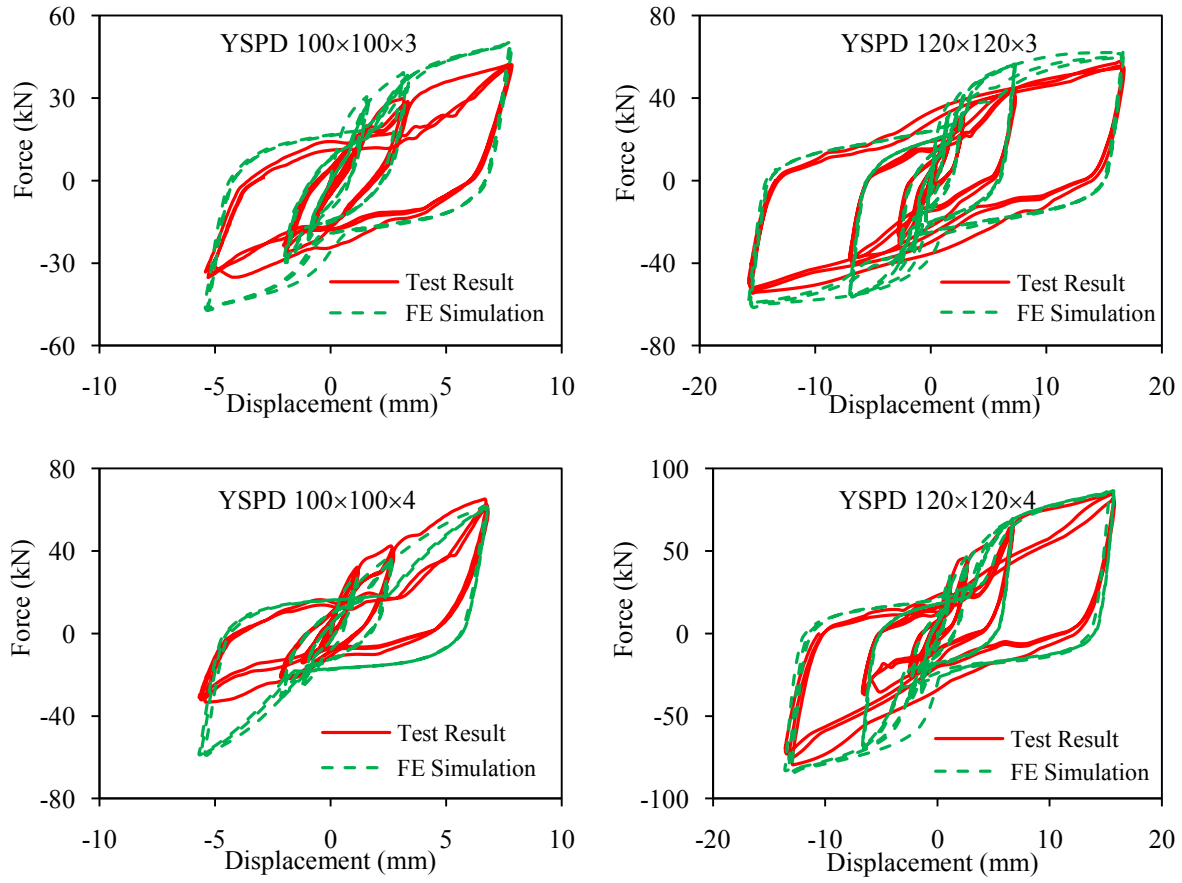

Figure 16. Cyclic responce of YSPDs

The energy dissipated in one cycle can be measured by calculating the area bounded by the cyclic response. Total energy dissipation for both test results and finite element simulation are calculated. Comparisons of energy dissipation with the cumulative number of cycles are plotted in Figure 17. The comparison shows that the developed FE models are able to predict the amount of energy absorbed with reasonable accuracy.

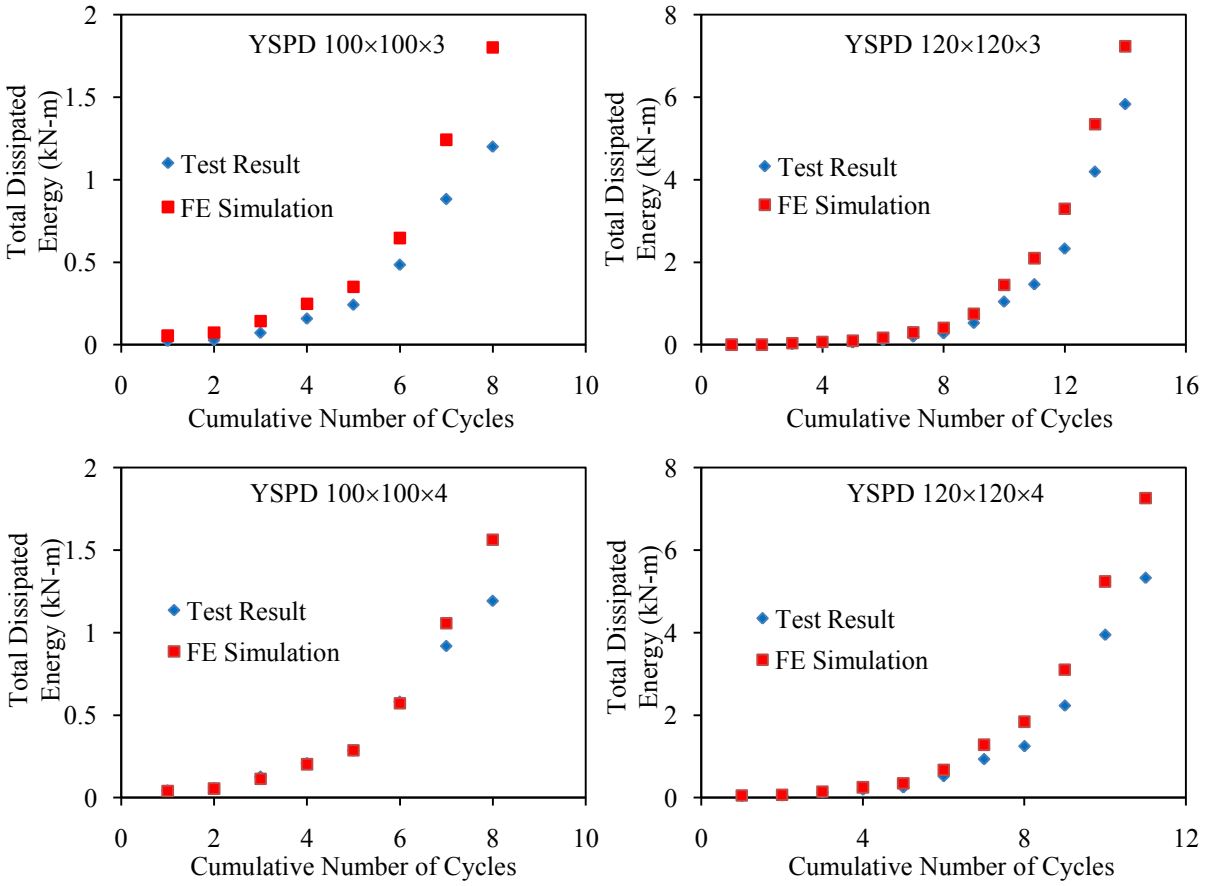

Figure 17. Comparison of hysteretic energy dissipation due to cyclic loading of YSPDs

6 CONCLUSION

Numerical modelling techniques for a newly proposed passive energy dissipation device YSPD is explained in detail, giving special significance of appropriate support conditions, initial geometric imperfections and residual stresses. Modelling of support conditions requires use of nonlinear spring elements with appropriate linear stiffness in both tension and compression. The out-of-plane rotation of the loading beam is observed to play a significant role in determining the initial slope of the load-deformation behaviour. Developed FE models were subjected to both monotonic and cyclic loading and the obtained results showed good agreement with the test results.

REFERENCES

[1] Chan, R. W. K., Albermani, F., and Williams, M. S., 2009, "Evaluation of Yielding Shear Panel Device for Passive Energy Dissipation," Journal of Constructional Steel Research, 65(2), pp. 260-268.

[2] Williams, M., and Albermani, F., 2003, "Monotonic and Cyclic Tests on Shear Diaphragm Dissipators for Steel Frames," Civil Engineering Bulletin No. 23, Department of Civil Engineering, University of Queensland, Australia.

[3] Schmidt, K., Dorka, U. E., Taucer, F., and Magnonette, G., 2004, "Seismic Retrofit of a Steel Frame and an Rc Frame with Hyde Systems," Institute for the Protection and the Security of the Citizen European Laboratory for Structural Assessment, European Commission Joint Research Centre.

[4] Williams, M., and Albermani, F., 2006, "Monotonic and Cyclic Tests on Shear Diaphragm Dissipators for Steel Frames," Advanced Steel Construction, 2(1), pp. 1-21.

[5] Chan, R. W. K., 2008, "Metallic Yielding Devices for Passive Dissipation of Seismic Energy," PhD Thesis, University of Queensland.

[6] Alinia, M. M., Gheitasi, A., and Erfani, S., 2009, "Plastic Shear Buckling of Unstiffened Stocky Plates," Journal of Constructional Steel Research, doi: 10.1016/j.jcsr.2009.04.001(

[7] Cen - European Committee for Standardization, 2006, "En 1993-1-5. Eurocode 3: Design of Steel Structures, Part 1.5: Plated Structural Elements."

[8] Ansys, "Ansys 11.0 Documentation," ANSYS Inc., Southpointe, 275 Technology Drive, Canonsburg, PA 15317.

[9] De Matteis, G., Formisano, A., Panico, S., and Mazzolani, F. M., 2008, "Numerical and Experimental Analysis of Pure Aluminium Shear Panels with Welded Stiffeners," Computers & Structures, 86(6), pp. 545-555.

[10] Soo Kim, T., and Kuwamura, H., 2007, "Finite Element Modeling of Bolted Connections in Thin-Walled Stainless Steel Plates under Static Shear," Thin-Walled Structures, 45(4), pp. 407-421.

[11] Ashraf, M., Gardner, L., and Nethercot, D. A., 2006, "Finite Element Modelling of Structural Stainless Steel Cross-Sections," Thin-Walled Structures, 44(10), pp. 1048-1062.

[12] Ellobody, E., and Young, B., 2005, "Structural Performance of Cold-Formed High Strength Stainless Steel Columns," Journal of Constructional Steel Research, 61(12), pp. 1631-1649.

[13] Dawson, R., and Walker, A., 1972, "Post-Buckling of Geometrically Imperfect Plates," Journal of the Structural Division, 98(1), pp. 75-94.

[14] Gardner, L., 2002, "A New Approach to Structural Stainless Steel Design," PhD. thesis. Structures Section, Department of Civil and Environmental Engineering. Imperial College London, UK.

[15] Schafer, B., and Pekoz, T., 1998, "Computational Modeling of Cold-Formed Steel: Characterizing Geometric Imperfections and Residual Stresses," Journal of Constructional Steel Research, 47(3), pp. 193-210.

[16] Zhang, Y. C., Wang, C. G., and Zhang, Z. N., 2007, "Tests and Finite Element Analysis of Pin-Ended Channel Columns with Inclined Simple Edge Stiffeners," Journal of Constructional Steel Research, 63(3), pp. 383-395.

[17] Sun, J., and Butterworth, J., 1998, "Behaviour of Steel Single Angle Compression Members Axially Loaded through One Leg," In: Proceedings of the Australian structural engineering conference, Auckland, pp. 859-66.

[18] Pokharel, N., and Mahendran, M., 2004, "Finite Element Analysis and Design of Sandwich Panels Subject to Local Buckling Effects," Thin-Walled Structures, 42(4), pp. 589-611.

[19] Pavlovcic, L., Detzel, A., Kuhlmann, U., and Beg, D., 2007, "Shear Resistance of Longitudinally Stiffened Panels - Part 1: Tests and Numerical Analysis of Imperfections," Journal of Constructional Steel Research, 63(3), pp. 337-350.

[20] Masubuchi, K., 1980, Analysis of Welded Structures : Residual Stresses, Distortion, and Their Consequences, Pergamon Press, Oxford ; New York.

[21] Odar, E., Nishino, F., and Tall, L., 1967, "Residual Stresses in Welded Built-Up "T-1" Shapes," WRC Bulletin, 121(April), pp. 22-29.

[22] Murugan, N., and Narayanan, R., 2009, "Finite Element Simulation of Residual Stresses and Their Measurement by Contour Method," Materials and Design, 30(6), pp. 2067-2071.

[23] Cruise, R., and Gardner, L., 2006, "Measurement and Prediction of Geometric Imperfections in Structural Stainless Steel Members," Structural Engineering and Mechanics, 24(1), pp. 63-89.

[24] European Convention for Constructional Steelwork, E., 1984, "Ultimate Limit State Calculation of Sway Frames with Rigid Joints," Technical Committee 8 - Structural Stability Technical Working Group 8.2 - System.

[25] Ueda, Y., Yasukawa, W., Yao, T., Ikegami, H., and Ohminami, R., 1975, "Effect of Welding Residual Stresses and Initial Deflection on Rigidity and Strength of Square Plates Subjected to Compression (Report I)," Trans, of JWRI, 4(2), pp. 29-43.

[26] Liang, Q., and Uy, B., 2000, "Theoretical Study on the Post-Local Buckling of Steel Plates in Concrete-Filled Box Columns," Computers and Structures, 75(5), pp. 479-490.